Synaptic Complex Formation of Two Retrovirus DNA Attachment Sites by Integrase: A Fluorescence Energy Transfer Study†

Sibes Bera,*,‡ Ajaykumar C. Vora,‡ Roger Chiu,‡ Tomasz Heyduk,§ and Duane P. Grandgenett‡

Institute for Molecular Virology and Department of Biochemistry and Molecular Biology, St. Louis University Health Sciences Center, St. Louis, Missouri 63110

Received May 5, 2005; Revised Manuscript Received July 12, 2005

ABSTRACT: The integration of retroviral DNA by the viral integrase (IN) into the host genome occurs via assembled preintegration complexes (PIC). We investigated this assembly process using purified IN and viral DNA oligodeoxynucleotide (ODN) substrates (93 bp in length) that were labeled with donor (Cy3) and acceptor fluorophores (Cy5). The fluorophores were attached to the 5′ 2 bp overhangs of the terminal attachment (att) sites recognized by IN. Addition of IN to the assay mixture containing the fluorophore-labeled ODN resulted in synaptic complex formation at 14 °C with significant fluorescence resonance energy transfer (FRET) occurring between the fluorophores in close juxtaposition (from ∼15 to 100 Å). Subsequent integration assays at 37 °C with the same ODN (^{32}P-labeled) demonstrated a direct association of a significant FRET signal with concerted insertion of the two ODNs into the circular DNA target, here termed full-site integration. FRET measurements (ΔF) show that IN binds to a particular set of 3′ OH recessed substrates (type I) generating synaptic complexes capable of full-site integration that, as shown previously, exhibit IN mediated protection from DNaseI digestion up to ∼20 bp from the ODN att ends. In contrast, IN also formed complexes with nonspecific DNA ends and loss-of-function att end substrates (type II) that had significantly lower ΔF values and were not capable of full-site integration, and lacked the DNaseI protection properties. The type II category may exemplify what is commonly understood as "nonspecific" binding by IN to DNA ends. Two IN mutants that exhibited little or no integration activity gave rise to the lower ΔF signals. Our FRET analysis provided the first direct physical evidence that IN forms synaptic complexes with two DNA att sites in vitro, yielding a complex that exhibits properties comparable to that of the PIC.

Integration of retroviral DNA by integrase (IN)[1] into the host chromosome is an essential step in virus replication. IN multimers are associated with both ends of the linear viral cDNA in the PIC where several other viral and cellular proteins are also found (*1*−*6*). For most retroviruses, two nucleotides are removed from both 3′-terminal blunt-ended DNA att sites by IN (3′-OH processing), exposing the highly conserved CA dinucleotide at the recessed ends. The 3′ ends of the viral DNA undergo IN-mediated integration into genomic DNA in a concerted fashion (termed concerted or full-site integration). The integration process is completed by cleavage of the unpaired dinucleotides from the 5′ ends of viral DNA and host-mediated repair of the gaps between the viral and genomic DNA, resulting in a short duplication of cellular DNA sequences (*7*). The sizes of the duplications (4−6 bp) are dependent upon the specific retrovirus species. The distances between the recessed 3′-OH ends held together by IN must be in the range of ∼16−20 Å prior to integration to allow these size duplications (*7*) (Figure 1).

Structural investigations have shown that IN possesses three distinct domains (*8*−*13*). The N-terminal domain (∼50 residues) is characterized by a zinc-stabilized helix−turn−helix motif. The central domain (∼180 residues), also called the catalytic core, contains the D,D(35)E motif conserved among retroviral and retrotransposon IN (*14*). This motif is essential for catalysis, and single mutations in the three D,D-(35)E residues impair enzymatic functions. The core domain is also involved in binding to the viral DNA att site and target DNA sequences. The C-terminal domain (∼50 residues) of IN possesses nonspecific DNA binding properties and is involved in stabilizing IN−DNA complexes. The central and C-terminal domains are also involved in the formation of dimers and tetramers (*15*). Even though the structures of the three domains have been determined individually or in two domain pairs, their spatial arrangements in synaptic complexes composed of full-length IN with att DNA substrates are unknown.

Several models describing the arrangement of IN−viral DNA complexes alone or with cellular DNA have been proposed on the basis of biochemical and structural ap-

† This work was supported in part by National Institutes of Health Grants CA16312 and AI31334.

* To whom correspondence should be addressed. Phone: (314) 977-8786. Fax: (314) 977-8798. E-mail: beras@slu.edu.

‡ Institute for Molecular Virology.

§ Department of Biochemistry and Molecular Biology.

[1] Abbreviations: PIC, preintegration complexes; IN, integrase; att, attachment site; ds, double-stranded DNA; ss, single-stranded DNA; wt, wild type; ODN, oligodeoxynucleotide; NS, nonspecific; FRET, fluorescence resonance energy transfer; DNaseI, deoxyribonuclease I; AMV, avian myeloblastosis virus; RSV, Rous sarcoma virus; HEPES, *N*-(2-hydroxyethyl)piperazine-*N*′-2-ethanesulfonic acid; DTT, dithiothreitol; LTR, long terminal repeats; Cy3 and Cy5, cyanine maleimide dyes.

10.1021/bi0508340 CCC: $30.25
Published on Web 10/29/2005

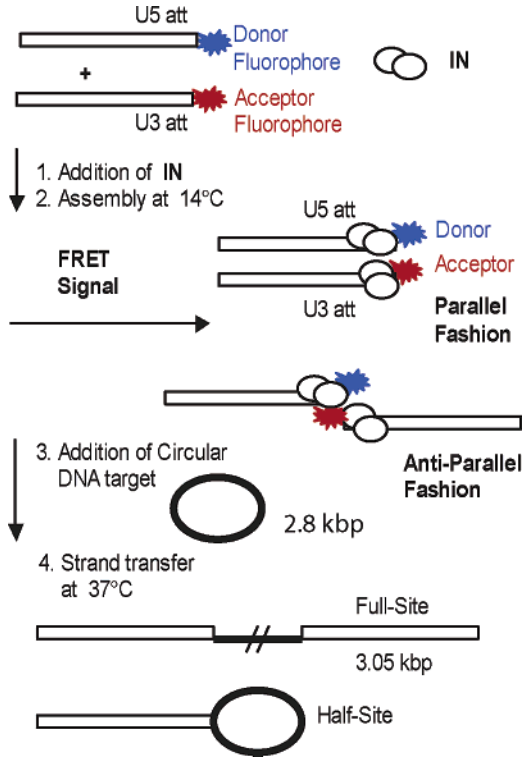

FIGURE 1: Schematic for assembly and FRET analyses of IN−att DNA synaptic complexes that are capable of full-site integration. The U5 and U3 att ODNs are labeled with donor (blue) and acceptor (red) fluorophores, respectively. IN is depicted as a dimer. In steps 1 and 2, assembly of the synaptic complexes occurs at 14 °C, allowing the assessment of the synaptic complex formation without strand transfer activity. The U5 and U3 att sites are modeled in either a parallel (*12*, *16*, *17*) or an antiparallel (*13*) fashion. The number of IN subunits is unknown, and a tetramer is only shown for illustrative purposes. In steps 3 and 4, the assembled synaptic complexes are also subjected to strand transfer analysis at 37 °C by the addition of supercoiled DNA. Two integration products are produced. The full-site products are produced when two individual donor substrates are inserted into the target DNA in a concerted fashion, producing the linear 3.1 kb product. The half-site product is produced when IN inserts only one donor molecule into the target.

proaches (Figure 1) (*12*, *13*, *16*, *17*). In one model, the U5 and U3 att DNA sites are in a parallel configuration (Figure 1) and are held together by a tetramer or an octamer of IN. Each viral DNA end interacts with an active site and the C-terminal domain donated by the same IN dimer, while the entire synaptic complex is held together by interactions between IN subunits in trans. In another model, the viral DNA ends are held together in an antiparallel fashion (Figure 1) with the active site and C-terminal domains supplied in trans to each DNA end by the two IN dimers. With both models, the 3′-OH recessed U5 and U3 att site ends must be within ∼16−20 Å for insertion of the viral ends into the target DNA. Using only purified IN and viral DNA substrates, we investigated the process through which synaptic complexes assemble in a way which would not rely upon full-site integration activity. To achieve this, we took advantage of the distance requirements (∼18 Å) of U5 and U3 DNA ends held together by IN in synaptic complexes capable of full-site integration. The placement of Cy3 and Cy5 fluorophores separately at the ends of the att DNA substrates would allow energy transfer between the fluorophores held together by IN in synaptic complexes (Figure 1). By FRET measurements, we investigate these interactions containing the fluorophore-labeled ODN and IN by quantifying the energy transfer occurring between the fluorophores in close juxtaposition (*18*, *19*).

We investigated the assembly properties of IN−DNA synaptic complexes at 14 °C using FRET. We positively correlated significant fluorescence signal (ΔF) changes with full-site integration activity at 37 °C and protection of the ∼20 bp region of active att site sequences by IN from DNaseI digestion at 14 °C (*20*, *21*). The fluorescence intensity changes allowed us to identify two types of IN−DNA complexes, one rising from active att DNA substrates and the other from non-active att site DNA substrates. For example, a single-nucleotide change in active wt U3 att sequences at position 7 (C to A) prevented full-site integration activity and DNaseI protection by IN (*22*) as well as a significant FRET signal. Our FRET analysis provides the first direct evidence that IN associates with two att site DNA substrates, forming complexes in vitro whose integration capacity is comparable to that of the PIC.

EXPERIMENTAL PROCEDURES

Purification of RSV IN and Its Mutants. Recombinant wt RSV IN and several IN mutants (D121A and W233A) were purified to near homogeneity (*23*). Fractions from the final purification step were divided into aliquots and stored at −70 °C. IN dilution buffer was 50 mM HEPES-NaOH (pH 7.5), 3 mM DTT, 1 mM EDTA, 10 mM $MgCl_2$, 10% glycerol, and 0.8 M NaCl. Protein concentrations were determined by absorbance at 280 nm, where 1 OD unit corresponds to a concentration of 0.54 mg/mL (*23*). Molar concentrations were calculated as IN dimers (64 μg/mL is equal to 1000 nM).

Oligonucleotides. To provide structure−function relationships between substrates for full-site integration activities with fluorophore-labeled substrates using FRET, we designed a series of ODNs that could be used for both experimental approaches (Figure 2). Dual PAGE-purified unlabeled synthetic ODNs (91 and 93 bases) with U3 and U5 LTR att sequences and nonspecific (NS) sequences of pGEM origin were purchased from Qiagen. The U5 and U3 LTR sequences were Schmidt-Ruppin strain A. The gain of function ("G") U3 substrates (Figure 2, sequences c and d) with an A mutated at position 6 on the catalytic strand increased its strand transfer activities over those of wt U3 and wt U5 (*20*). The loss-of-function ("L") U3 substrate contained a C to A mutation at position 7 on the catalytic strand (Figure 2, sequences 4−6). The 5′ end fluorescently labeled (Cy3 or Cy5) ODNs (93 bases, dual HPLC purified) were purchased from Integrated DNA Technologies, Inc. (Figure 2). The degree of fluorophore labeling of DNA was determined on the basis of the ratio of attached fluorophore to DNA concentration. The ratios were ∼0.8 for all ODNs used in this study.

For strand transfer assays, single-stranded ODNs (93-base noncatalytic strand) were 5′ end-labeled with [γ-^{32}P]ATP using T4 polynucleotide kinase (Figure 2). The radioactive ODNs were hybridized with equimolar unlabeled 91-base complementary catalytic strands. The mixtures were heated to 90 °C for 5 min followed by annealing with slow cooling to room temperature (90 min). The completeness of DNA hybridization was checked by electrophoresis of DNA on

Strand Transfer Substrates

a) wt U3
5'-..... GTATTGCATAAGACTACA
3'-.....CATAACGTATTCTGATGTAT-^{32}P

b) wt U3-Cy5
^{32}P-5'-.....GTATTGCATAAGACTACA
3'-.....CATAACGTATTCTGATGTAT-Cy5

c) G U3
5'-.....GTATTGCATAAGACAACA
3'-.....CATAACGTATTCTGTTGTAT-^{32}P

d) G U3-Cy5
^{32}P-5'-.....GTATTGCATAAGACAACA
3'-.....CATAACGTATTCTGTTGTAT-Cy5

e) wt U5
5'-.....ATGAAGCAGAAGGCTTCA
3'-.....TACTTCGTCTTCCGAAGTAT-^{32}P

f) wt U5-Cy3
^{32}P-5'-.....ATGAAGCAGAAGGCTTCA
3'-.....TACTTCGTCTTCCGAAGTAT-Cy3

Paired Fluorophore Substrates

ODN pairs	Fluorophore acceptor	Fluorophore donor	Category
1	wt U3-Cy5	wt U5-Cy3	Type I
2	G U3-Cy5	wt U5-Cy3	
3	wt U5-Cy5	wt U5-Cy3	
4	L U3-Cy5	wt U5-Cy3	
5	L U3-Cy5	L U3-Cy3	Type II
6	L U3-Cy5, blunt ended	L U3-Cy3, blunt ended	
7	NS-Cy5	NS-Cy3	
8	NS-Cy5, blunt ended	NS-Cy3, blunt ended	

FIGURE 2: ODN used for strand transfer and FRET studies. At the top are some of the DNA substrates (a−f) used for strand transfer activities. The wt U3 (a and b), wt U5 (e and f), and G U3 (c and d) mutants are shown with ^{32}P at the 5′ end without and with attached fluorophores, respectively. The G U3 att DNA had an A (bold) instead of a T at position 6 on the catalytic strand. With the fluorophore present, the complementary catalytic strand was labeled with ^{32}P on its 5′ end prior to annealing. Numbering was from the blunt end of the substrates. The catalytic and noncatalytic strands were 91 and 93 nucleotides in length, respectively. At the bottom are the matched pairs of fluorophore acceptor and donor substrates (pairs 1−8) used in this study. The NS DNA (93 base) sequences were taken from the pGEM-3 vector (positions 119−211) as nonspecific DNA. The fluorophore pairs were separated into type I and type II relative to their fluorescence intensity signal (on the right under category) (Figure 5).

2% SeaPlaque agarose gels. ODNs were hybridized (>95%), and no further purification was required for strand transfer or fluorescence assays.

For fluorescence studies, ds fluorophore-modified ODNs were generated by hybridization of fluorophore 5′-labeled 93-base noncatalytic DNA strands with nonlabeled 91-base catalytic strands (Figure 2, bottom). The donor fluorophore Cy3 was generally attached to the wt U5 93-base ODN, while the acceptor Cy5 was attached to either wt U3 or G U3. Other combinations of fluorophore attachments to the 5′ ends of DNA are described in the text. Fluorophore-labeled ODNs (93 bases) were also hybridized to 91-base ODNs that were labeled with ^{32}P at their 5′ ends (Figure 2, sequences b, d, and f) to determine if the fluorophore labeling affected strand transfer activity. Blunt-ended DNA and mutant DNA substrates for FRET and strand transfer were produced in a similar manner.

Integration Assays. Conditions for assembling nucleoprotein complexes capable of producing more full-site integration products over half-site integration products were previously established (*24*). Full-site integration is the concerted insertion of two ODNs into a target, while half-site integration is the insertion of one ODN into a target (Figure 1). Optimal conditions were 20 mM HEPES (pH 7.8), 250 mM NaCl, 10% DMSO, 10 mM $MgCl_2$, 1 mM DTT, and 8% polyethylene glycol (6000 Da). Reaction mixtures containing various amounts of RSV IN and 15 ng of ds ODN (2.5 nM) per 100 μL were preincubated at 14 °C for 30 min to assemble synaptic complexes. To initiate strand transfer, 5 μg of supercoiled pGEM3 target DNA of 2.86 kb (1:10 ODN:target molar ratio) was added to the mixture followed by immediate incubation at 37 °C for 30 min. The reactions were stopped by addition of proteinase K, EDTA, and SDS. The DNA products were subjected to electrophoresis on 1.5% agarose gels. The full-site products produced with the ODN were 3.05 kb in length as determined by comparison to a 1 kb linear DNA ladder (Promega). An Amersham Biosciences PhosphorImager was used to determine the quantities of each product. The presented data represent triplet measurements with error bar analysis.

Steady-State Fluorescence Measurements. Equimolar amounts of 3′-OH recessed ODN substrates labeled with donor (Cy3) and acceptor (Cy5) fluorophores were mixed in the optimal strand transfer reaction mixture on ice. The samples were equilibrated at 14 °C prior to the addition of IN for analysis. All fluorescence measurements were performed on either an Amino-Bowman (Spectronic Instruments, Rochester, NY) Series 2 or a Fluoromax-3 (Jobin Yvon, Inc., Edsion, NJ) spectrofluorometer with a temperature-regulated cell holder. The band-pass was 4 nm each for excitation and emission monochromator. The samples were excited at 550 nm (λ_{ex} for Cy3), and fluorescence emission spectra were collected from 640 to 720 nm (λ_{em}^{max} for Cy5 is ~668 nm) using semimicro quartz cell (volume of 200 μL). Other att site and non-att site ODN substrates were handled in a similar manner. All spectra and emission intensity values were corrected for buffer and instrument. The presented data represent triplet measurements with error bar analysis.

Analysis of Donor−Target Recombinants. Construction and radioactive labeling of the 474 bp DNA substrates containing an internal SupF gene, a genetic selection marker, with 3′-OH recessed wt U3 and wt U5 ends were described (*25*−*27*). Digestion of 474 bp DNA with a unique internal TfiI site produced 243 bp single-ended U3 and 231 bp U5 att DNA ODN substrates. A similar 474 bp DNA substrate containing G U3 with wt U5 ends was also used. The correct size full-site DNA integration products were isolated, ligated, and transformed into MC1061/P3 cells (*28, 29*). Colonies were screened for plasmids that were analyzed by size, restriction enzyme digestions (BglII, EcoRI, and BamHI), and DNA sequencing for donor−target junction. Sequencing analysis of full-site integration products that were produced by three independent reactions was performed.

RESULTS

Optimized Solution Conditions for Assembly of Synaptic Complexes and Full-Site Integration. Strand transfer assays were performed to confirm solution conditions (*24*) and concentrations of different reaction components to maximize full-site integration. For these studies, we used the G U3 substrate (Figure 2, sequence c). Protein titration experiments established that the optimum molar ratio of IN to G U3 was approximately 6:1 (Figures 1S and 2S of the Supporting Information). The optimum assembly time for synaptic complex formation was ~10 min at 14 °C (Figure 3).

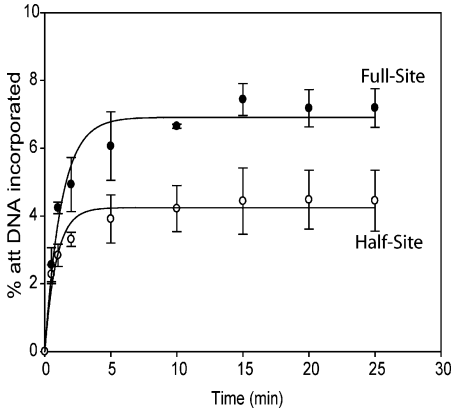

FIGURE 3: Kinetics of assembly of nucleoprotein complexes for paired G U3−Cy5 and U5−Cy3 ODNs with IN. ^{32}P-labeled ODNs (1.25 nM each) containing fluorophores (Figure 2, sequences d and f) were mixed and assembled with 18 nM IN at 14 °C for 30 min. Target DNA was added followed by strand transfer at 37 °C for 30 min. The products were analyzed as described in Experimental Procedures. The solid line represents the best fit with a single-exponential growth equation.

The standard strand transfer assay contained 2.5 nM ODN and 13 nM IN. We anticipated for our FRET studies that higher ODN concentrations were necessary to effectively assess resonance energy transfer between acceptor and donor fluorophores attached to the 5′ end of the ODN. Therefore, we tested a wide range of concentrations of IN and ODN from the above concentrations up to 20 nM ODN and 104 nM IN. The same percentages of full-site and half-site products were obtained which suggests the concentrations of components did not affect product formation (data not shown). Therefore, ODN and IN at these higher concentrations were used to facilitate FRET measurements.

Sequencing of ODN Donor−Target Junctions Produced by RSV IN. We and others have established that the avian IN has the capacity to produce the correct 6 bp host site duplications upon full-site integration with high fidelity (*20*, *25*, *27*−*30*). To investigate the fidelity of the host site duplications under our new conditions with RSV IN, we tested whether two slightly larger ODNs (∼240 bp) containing either wt U3 and wt U5 ends or G U3 and wt U5 ends produced the correct integration products. Plasmid DNA from individual colonies was isolated and sequenced (Table 1S of the Supporting Information). All of the sequenced DNA clones exhibited the correct host site duplications with a high fidelity upon full-site integration.

Integration Assays of Fluorophore-Labeled ODN. The possibility that Cy3 and Cy5 fluorophores attached to the ODN at their att site ends would inhibit strand transfer activities existed. We use G U3 and G U3−Cy5 (Figure 2, sequences c and d, respectively) as well as wt U5 and wt U5−Cy3 (Figure 2, sequences e and f, respectively) to test this possibility. With both sets of ODNs, the full-site integration activity with the fluorophore-modified ODN were reproducibly higher than that with the corresponding ODN without the fluorophore (Figure 3S of the Supporting Information). Half-site integration activities were also similarly increased (data not shown). The significantly higher strand transfer activities observed with the G U3 substrates over wt U5 have been observed previously (*20*, *25*). To test the interactions of G U3−Cy5 and wt U5−Cy3 for full-site integration, we mixed equimolar quantities of both fluorophore-labeled ODNs that were also labeled with ^{32}P on the complementary strand (Figure 2, sequences d and f). Strand transfer analysis showed a typical assembly process and yield of full-site and half-site products for G U3−Cy5 and U5−Cy3 (Figure 3). The results suggest that the fluorophores attached to the 5′ ends of ODNs containing att sites do not interfere with assembly of synaptic complexes by IN capable of full-site integration.

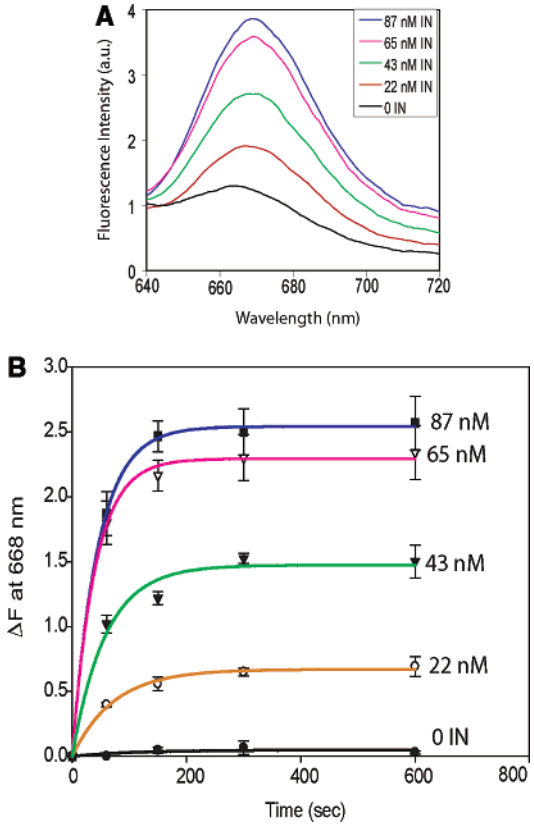

FIGURE 4: Sensitized fluorescence emission spectra (FRET) of the acceptor fluorophore (G U3−Cy5) mixed with an equimolar amount of the donor fluorophore (wt U5−Cy3) titrated with IN. (A) Each fluorophore-labeled ODN (6.25 nM each) (Figure 2, pair 2) was mixed and assembled at 14 °C with IN at 0, 22, 43, 65, and 87 nM. The excitation wavelength was 550 nm (λ_{ex} = 550 nm for Cy3) with a 4 nm band-pass for each excitation and emission monochromator. Spectra presented in the figure were taken 10 min after addition of IN with buffer corrected. Emission maxima were observed at around 668 nm (λ_{em} = 668 nm for Cy5). (B) The data showed the effect of IN concentration (0−87 nM) on the kinetics of assembly of wt U5−Cy3 mixed with G U3−Cy5 at 668 nm ($\Delta F = F_{oligo+IN} - F_{oligo}$) was due to excitation of U5−Cy3 at 550 nm plotted with time. Each set of data was then fitted with the single-exponential growth equation $\Delta F = \Delta F_{max}[1 - \exp(-kt)]$, where ΔF_{max} is the maximum fluorescence intensity change at that IN concentration and k is the rate constant.

Steady-State Fluorescence Studies. To investigate assembly of IN−DNA synaptic complexes at 14 °C, we mixed equimolar quantities (6.25 nM each) of G U3−Cy5 (acceptor) and wt U5−Cy3 (donor) (Figure 2, pair 2) in the presence of varying IN concentrations (Figure 4A). The increasing observed fluorescence emission intensity spectra of the acceptor fluorophore with increasing concentrations of IN strongly suggest that IN is capable of forming synaptic complexes wherein the excited donor fluorophore is transferring resonance energy to the acceptor fluorophore. The fluorescence intensity in the wavelength region from 640 to 720 nm increased approximately 4-fold (maximum at 668

nm) with a saturating concentration of IN of 87 nM. The increase in the sensitized emission of G U3−Cy5 at 668 nm (Figure 4B, ΔF) due to excitation of U5−Cy3 at 550 nm shows the formation of synaptic complexes with time at different IN concentrations. In the absence of IN, there was no fluorescence intensity change upon mixing the donor and acceptor ODN together. The nature of the assembly kinetics monitored by resonance energy transfer was similar to the nature of the assembly kinetics observed for full-site integration activity (Figure 3). The fluorescence intensity signals observed with the ODN synaptic complexes were stable for at least 40 min at 14 °C; similar stability was observed for synaptic complexes with 3.6 kb DNA (*20*). The results suggest IN holds two att ends together in synaptic complexes capable of mediating full-site integration.

To further establish that energy transfer occurred between the donor ODN (U5−Cy3) and the acceptor ODN (G U3−Cy5) upon addition of IN, a series of additional control assays were performed. In the presence of both fluorophore substrates, different amounts of IN were added as described in the legend of Figure 4. In one experiment, the donor was excited (550 nm), while in another, the acceptor was excited (648 nm). The emission fluorescence intensities were monitored in the regions of 560−720 and 655−720 nm, respectively. No fluorescence intensity changes were observed upon addition of IN when the acceptor fluorophore was excited (data not shown). However, during the excitation of the donor fluorophore, intensity changes occurred. The fluorescence emission intensity of the acceptor molecule (G U3−Cy5) increased in the 640−720 nm region (Figure 4A) at the cost of the donor molecule (U5−Cy3) in the 560−640 nm region, indicating resonance energy transfer occurring because of their interactions while forming synaptic complexes. Quenching of the donor fluorophore occurred in the broad low-wavelength region in comparison to the sensitized emission of the acceptor fluorophore. The sensitized emission intensity was measured (ΔF at 668 nm) instead of quenching because the former gave a 4-fold stronger signal.

The assembly of IN−ODN synaptic complexes capable of full-site integration activity required the presence of PEG and 10% DMSO (*24*). We determined whether the presence of these cosolvents also affected the assembly of the synaptic complexes as measured by FRET. A series of FRET experiments were performed in the absence and presence of these reagents using IN with G U3−Cy5 and U5−Cy3 (Figure 2, pair 2). With both PEG and DMSO present as normal (Figure 4), the maximum ΔF value was set to 100%. Without PEG but with DMSO, the FRET signal (ΔF) was 1% of the maximum (data not shown). With PEG but without DMSO, the ΔF was 32% of the maximum. The results suggest that both cosolvents contribute to assembly of the synaptic complexes by IN to varying degrees. The addition of Mg^{2+} was not necessary to obtain the normal enhanced ΔF upon assembly (data not shown). Similar effects were previously observed with the PEG and DMSO for full-site integration using ∼500 bp DNA substrates and AMV IN (*24*).

The ^{32}P-labeled U5−Cy3 and G U3−Cy5 fluorophore-labeled ODN (Figure 2, sequences d and f, respectively) gave rise to full-site products (Figure 3) that result from the formation of U3−target−U3, U5−target−U3, and U5−target−U5 reactions. Restriction enzyme digestions of full-site products produced with other viral donors show that the yield of the U3−target−U5 product is ∼36% (*25*, *34*). With our FRET measurements, only the interactions between U5−Cy3 (donor) and U3−Cy5 (acceptor) are measured in synaptic complexes. Therefore, approximately one-third of the synaptic complexes are producing energy transfer upon excitation of the donor fluorophore to the acceptor fluorophore with any of the pair of ODN substrates. The donor−donor and acceptor−acceptor fluorophore ODNs paired by IN which are ∼10 and ∼54% (*25*, *34*), respectively, do not provide a transfer energy fluorescence signal.

We also determined that the observed ΔF values of different assembled IN−ODN synaptic complexes were stable with time and upon centrifugation of the samples. Samples were prepared as described in the legend of Figure 4, where varying concentrations of IN were assembled with either U5−Cy3 and G U3−Cy5 or NS donor and its acceptor ODN. The samples were assembled at 14 °C for 15 min, and the ΔF was determined. These samples (400 μL each) were then subjected to centrifugation at 14 °C for 15 min at 8000*g*. Aliquots were carefully taken from the top of the tubes and then again subjected to FRET measurement. The total elapsed time between the initial FRET readings and the final readings was 40 min. The ΔF was stable with all four IN concentrations that were tested with either U5−Cy3 and G U3−Cy5 synaptic complexes or IN−NS DNA complexes (data not shown). The results suggest that the IN−ODN synaptic complexes were stable and did not form large insoluble structures in solution.

Specificity of Synaptic Complex Formation. IN appears to bind to closed DNA and DNA ends in a nonspecific manner as demonstrated by nitrocellulose filter binding assays and other approaches, although specific contacts of IN residues with att site sequences are observed by DNA−protein cross-linking studies (*7*, *26*, *31*). With AMV and RSV IN, the enzyme forms specific complexes at the ends of G U3 and wt U3 DNA substrates, producing an ∼20 bp DNaseI protective footprint at the att sites but not with L U3, wt U5 DNA, and nonspecific DNA ends (*20*−*22*). We wanted to determine by FRET whether RSV IN could differentiate between active att ends, mutant att ends, and nonspecific ends (Figure 2, bottom).

Eight pairs of ODNs labeled with donor and acceptor fluorophores were analyzed to investigate the specificity associated with synaptic complex formation. Figure 5 shows the maximum fluorescence intensity increase for different combinations of paired ODNs (Figure 2, pairs 1−8) with different concentrations of IN. In addition, we plotted the maximum change in resonance fluorescence intensity for the different pair sets of ODNs versus the ratio of IN dimer to DNA (Figure 4S of the Supporting Information). From these data, there appears to be two types (I and II) of ODNs for formation of complexes. For example, in type I, pairs 1−3 possess full-site integration activities, a fact which compares favorably with the observed increase in ΔF (Figure 5).

With paired ODNs observed in type II, none of the nucleoprotein complexes were capable of promoting full-site integration (Figure 5, Figure 6). The type II group contained the L U3 att site ODN (Figure 2, pairs 5 and 6) and the NS ODN (Figure 2, pairs 7 and 8). L U3 att DNA was shown to minimally promote half-site and full-site integration (data not shown). In addition, the type II blunt-

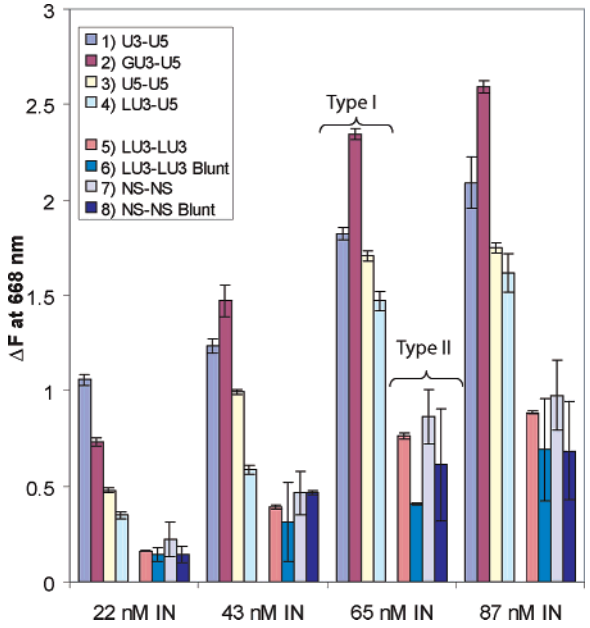

FIGURE 5: Relative synaptic complex formation of various paired fluorophore substrates with different IN concentrations. The maximum increase in sensitized emission intensity (ΔF) of the acceptor Cy5 fluorophore at 668 nm due to excitation of the donor Cy3 fluorophore at 550 nm is plotted against different combinations of fluorophore-labeled ODNs (see insert), also shown in the same order as in Figure 2. The increases in resonance energy transfer after 10 min were plotted as ΔF. Titrations of equimolar fluorophore-labeled donor and acceptor ODNs (6.25 nM each) with IN were performed as indicated at the bottom. The paired ODNs were categorized as type I or type II relative to their change in maximum fluorescence intensity.

ended ODNs were less effective in producing a significant signal than the same ODNs containing 3′-OH recessed ends (Figure 5). In summary, FRET was able to distinguish assembled complexes (pairs 1−3) that are capable of full-site integration from complexes (pairs 5−8) not capable of strand transfer activity.

Besides the type I group of paired ODNs (Figure 2, pairs 1−3) capable of full-site integration, it contains a pair of ODNs (Figure 2, pair 4) that comprised L U3 with wt U5. As shown in Figure 5, the L U3−L U3 ODN (pair 5) was in the type II category. Apparently, wt U5 was able to cooperate with L U3 to promote synaptic complex formation in the absence of significant strand transfer activities or DNaseI footprint protection at the L U3 att site (Figure 6) (*22*, *26*). The results suggest that at least with L U3−wt U5, assembly of synaptic complexes may be independent of catalysis. Trans interactions of att sites by IN for full-site integration have previously been observed in vitro (*32*−*34*) and in vivo (*3*, *35*, *36*).

To further distinguish type I from type II ODNs using FRET analysis, we attached Cy5 (acceptor) at the noncatalytic 5′ end of G U3 DNA, thereby producing another negative background control (Figure 1). The normal U5−Cy3 ODN containing the attached fluorophore at the att site was used as the donor fluorophore. We did not observe a FRET signal with a magnitude higher than that of the signal obtained from the NS ODN (data not shown), demonstrating that the donor and acceptor fluorophores must both be attached at the att sites and in close juxtaposition (from ∼15 to 100 Å) to produce a significant FRET signal.

The type II group contains fluorophore-labeled L U3−L U3 and NS DNA substrates in a 3′-OH recessed form as well as in a blunt-ended form. In both cases, the blunt-ended forms produced a less intense FRET signal than the 3′-OH recessed forms (Figure 5). Similar recessed and blunt-ended data were obtained with the type I substrates wt U3−U5 and G U3−U5 (data not shown). In a series of protein titration experiments, the ΔF decreases observed with blunt-ended substrates were ∼30% relative to the recessed substrates. The results suggest that IN has a higher affinity for 3′-OH recessed ends than for blunt ends (*7*).

RSV IN Mutants Exhibit Mutually Correlative Assembly Properties and Integration Capacities. We wanted to determine if several previously characterized RSV IN mutants were capable of forming synaptic complexes similar to wt recombinant RSV IN. We tested several concentrations of wt and mutant IN in assembling synaptic complexes (Figure 7). Recombinant RSV IN mutant D121E (catalytic core region) (*14*) and W233A (C-terminal region) (*21*) are catalytically inactive for strand transfer activities using G U3 (data not shown). wt RSV IN was capable of producing a significant FRET signal with G U3−Cy5 and wt U5−Cy3, while both mutants were only capable of producing a FRET signal equivalent to the signal obtained with NS ODN and wt RSV IN. The FRET data obtained from these two RSV IN mutants suggest these mutations prevent RSV IN from holding the two att sites sufficiently close in space to promote full-site integration. The results further suggest that both regions of IN are necessary for proper synaptic complex formation.

DISCUSSION

The structure of the PIC upon integration of the viral DNA genome into the host chromosome is not well defined. The ends of the viral genome must be within ∼18 Å of each other for IN to insert the DNA ends in a concerted fashion into the DNA target to produce the appropriate host site duplications. We labeled the 5′ ends of recessed ODN with Cy3 and Cy5 fluorophores to gain insight into the assembly process of synaptic complexes capable of full-site integration. FRET analysis provides the first direct physical evidence that IN is capable of holding together the U5 and U3 att DNA ends in trans, assembling synaptic complexes that exist prior to and independent of full-site catalysis.

The attachment of the Cy3 and Cy5 fluorophores to the 5′ ends of the two base overhangs at the att sites (Figure 2) does not hinder either half-site or full-site integration reactions (Figure 3S of the Supporting Information). The 5′ 2 bp overhangs interact with residues in the catalytic core (*13*, *16*), and these interactions apparently assist IN−viral DNA complexes in forming a stable "strand transfer" configuration (*32*, *37*−*39*). Our FRET studies also suggest that RSV IN preferentially recognizes substrates possessing recessed 3′-OH ends over blunt-ended substrate ends in assembling strand transfer complexes (Figures 5 and 6). The results support the possibility that IN requires a specific synaptic complex configuration for integration activity.

In the in vivo context of the PIC, only two DNA ends are available for binding to IN. In vivo (*3*, *40*, *41*) and in vitro studies (*20*, *25*, *30*, *34*) suggest that only the first ∼12 terminal nucleotides are critical for synaptic complex forma-

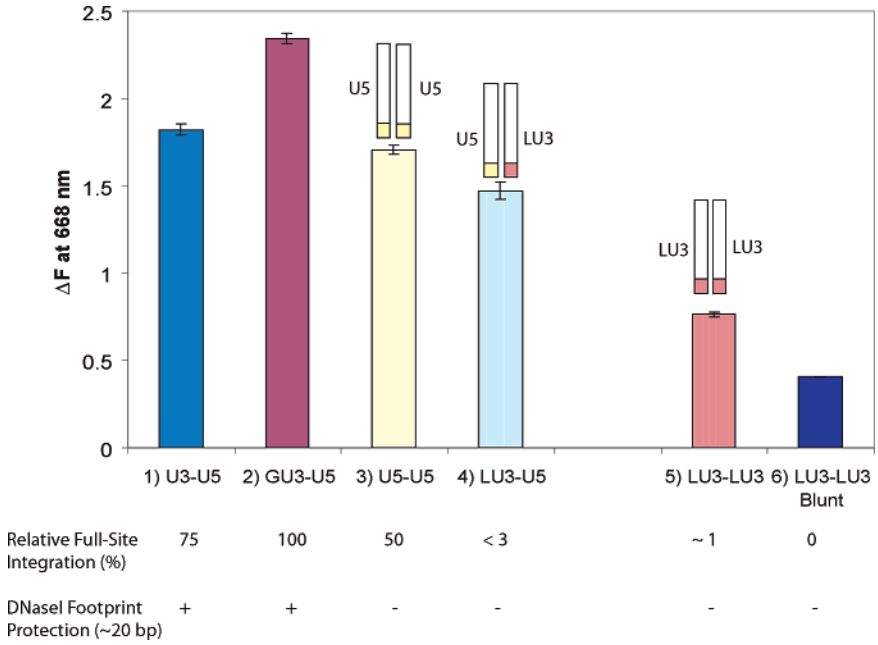

FIGURE 6: Positive correlation observed between synaptic complex formation using FRET with full-site integration and DNaseI footprint protection. ΔF_{max} at 668 nm was plotted for different pairs (Figure 2, pairs 1−6) (bottom of graph) of ODNs with 65 nM IN (from Figure 5). The relative degrees of full-site integration activities and DNaseI footprints obtained with linear 4 kb att DNA substrates (*20*−*22*, *25*) were shown at the bottom of each ODN pair. The relative full-site integration activities were set to equal 100% for G U3−U5 (wt U3−U5 as 75%, wt U5−U5 as 50%, and L U3−U5 as <3%). A plus sign means a positive footprint was obtained, whereas a minus sign means no detectable footprint. Tops of bars (insets, e.g., pairs 3−5) pictorially show the formation of synaptic complexes where two att ends are held together by IN.

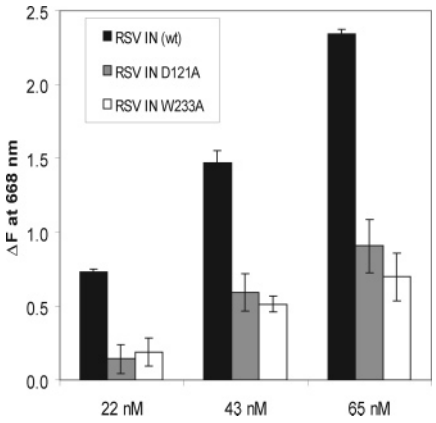

FIGURE 7: RSV IN mutants lack the ability to form integration-competent synaptic complexes. Fluorophore-labeled ODNs (6.25 nM each; G U3−Cy5 and wt U5−Cy3) (Figure 2, pair 2) were mixed and assembled at 14 °C, and the emission intensity was recorded at 668 nm before and after addition of IN (see Figure 4B). wt RSV and RSV IN mutants (D121A and W233A) were assayed at 22, 43, and 65 nM IN. The maximum increases in sensitized emission intensities (ΔF) at 668 nm were plotted for the different proteins indicated in the inserted box.

tion and full-site integration. However, IN binds to DNA ends in a nonspecific fashion in vitro and possesses multiple DNA binding sites (*7*, *42*−*44*). Our FRET measurements have allowed us to gain further insight into the DNA binding properties of IN. How does IN distinguish between att and non-att site sequences at the ends of DNA to allow both 3′-OH processing and strand transfer? DNA binding to blunt ends and subsequent 3′-OH processing studies have suggested that IN may preferentially interact with att sequences in a minor groove configuration (*45*). Our FRET studies suggest that IN binding to nonspecific ends, L U3 att ends, and blunt ends produces integration-incompetent type II IN−ODN complexes, in contrast to 3′-OH recessed att ends, which produce integration-competent type I ODN complexes. The type II category may constitute what is commonly understood as nonspecific binding of IN to DNA ends, thus explaining the background FRET signals with these ODNs. Simple binding of IN (type II complexes) to att blunt ends may allow for 3′-OH processing. Our results suggest IN has a higher affinity and a more stable configuration with 3′-OH recessed ends (Figure 6). This more stable configuration of IN may be a required for the generation of an integration-competent synaptic complex. Previous studies show that IN does not stably associate with the G U3 blunt-ended att site, and does not generate the ~20 bp DNaseI footprint observed with the 3′-OH recessed G U3 substrate (*20*). Since the 3′-OH processing of the blunt-ended DNA in the PIC is temporal and occurs within several hours of infection of the cells, the association of IN with the 3′-OH recessed viral ends probably assists in the formation of stable PIC both in vivo and in vitro (*1*, *2*, *46*, *47*).

In the context of the PIC, it appears that IN-bound 3′-OH recessed U5 and U3 termini must associate in trans, forming synaptic complexes capable of full-site integration; this mechanism bears analogy to other related DNA recombination systems (*3*). In vitro, IN bound to wt att 3′-OH recessed ends possesses the ability to interact with other wt or modified att sites in a way that promotes full-site integration (*26*, *33*, *34*). FRET analysis also supports the idea that IN acts in trans when bound to wt U5 and G U3 or other substrate combinations for assembly (Figure 6). Of particular interest is the ability of RSV IN to effectively promote the assembly of wt U5 (type I) with L U3 (type II), thus together producing a type I synaptic complex. Other experiments using either U3 or G U3 substrates with L U3 produced similar FRET data (data not shown). The results suggest that

although L U3 itself essentially lacks strand transfer activities (*22*, *26*), it is rescued by wt att site substrates, assembling type I integration-competent synaptic complexes, although with significantly lower integration activity. Possibly, at least with L U3, assembly of type I complexes with other wt att ODN substrates suggests that assembly can be independent of catalysis.

There is a positive correlation among the assembly of type I complexes with U3−U5 and G U3−U5 fluorophore combinations with full-site integration activities and DNaseI protection of ∼20 bp of att sequences at the ends of U3 and G U3 att substrates (Figure 6) (*20*−*22*). Previous studies demonstrate that although wt U5 is competent for full-site integration, no DNaseI footprints were observed up to ∼20 bp (*20*, *22*), suggesting that IN may bind differently to the U3 and U5 ends for full-site integration. Our FRET data clearly demonstrate that wt U5 promotes assembly of type I synaptic complexes as well as assisting the assembly of L U3 in an in trans fashion (Figures 5 and 6).

What properties are associated with integration-competent IN−DNA complexes that are capable of full-site integration in vitro? These complexes demonstrate a significant FRET signal (ΔF for type I substrates), in contrast to nonspecific type II substrates that give rise to only a background signal (Figure 5); they exhibit full-site integration activity (Figure 3), show a high fidelity for host site duplications, and give rise to protection (∼20 bp) from DNaseI at the att ends (Figure 6) (*20*). The stability and activities of the assembled synaptic complexes with ODN are similar to that observed with integration-competent synaptic complexes using 3.6 kb linear DNA substrates containing the same att site sequences (*20*). Precise distance measurements by time-resolved luminescence resonance energy transfer (LRET) (*48*) using appropriately labeled lanthanide donors and organic-based acceptors should permit better insights into the topology of the att DNA substrates within competent synaptic complexes (Figure 1).

ACKNOWLEDGMENT

We thank Jacob Zahm for his editorial comments.

SUPPORTING INFORMATION AVAILABLE

Agarose gel picture (Figure 1S) and analysis (Figure 2S) of strand transfer activities of G U3 at varying IN concentrations, the effect of attachment of a fluorophore to ODN on strand transfer activities (Figure 3S), the sequence analysis of att ODN−target junction sites (Table 1S), and the kinetics of formation of IN−DNA synaptic complexes (Figure 4S). This material is available free of charge via the Internet at http://pubs.acs.org.

REFERENCES

1. Brown, P. O., Bowerman, B., Varmus, H. E., and Bishop, J. M. (1987) Correct integration of retroviral DNA in vitro, *Cell 49*, 347−356.
2. Miller, M. D., Farnet, C. M., and Bushman, F. D. (1997) Human immunodeficiency virus type 1 preintegration complexes: Studies of organization and composition, *J. Virol. 71*, 5382−5390.
3. Chen, H., and Engelman, A. (2001) Asymmetric processing of human immunodeficiency virus type 1 cDNA in vivo: Implications for functional end coupling during the chemical steps of DNA transposition, *Mol. Cell. Biol. 21*, 6758−6767.
4. Wei, S. Q., Mizuuchi, K., and Craigie, R. (1998) Footprints on the viral DNA ends in moloney murine leukemia virus preintegration complexes reflect a specific association with integrase, *Proc. Natl. Acad. Sci. U.S.A. 95*, 10535−10540.
5. Suzuki, Y., and Craigie, R. (2002) Regulatory mechanisms by which barrier-to-autointegration factor blocks autointegration and stimulates intermolecular integration of Moloney murine leukemia virus preintegration complexes, *J. Virol. 76*, 12376−12380.
6. Piller, S. C., Caly, L., and Jans, D. A. (2003) Nuclear import of the pre-integration complex (PIC): The achilles Heel of HIV? *Curr. Drug Targets 4*, 409−429.
7. Brown, P. O. (1997) Integration, in *Retroviruses* (Coffin, J. M., Hughes, S., and Varmus, H., Eds.) pp 161−203, Cold Spring Harbor Laboratory Press, Plainview, NY.
8. Dyda, F., Hickman, A. B., Jenkins, T. M., Engelman, A., Craigie, R., and Davies, D. R. (1994) Crystal structure of the catalytic domain of HIV-1 integrase: Similarity to other polynucleotidyl transferases, *Science 266*, 1981−1986.
9. Bujacz, G., Jaskolski, M., Alexandratos, J., Wlodawer, A., Merkel, G., Katz, R. A., and Skalka, A. M. (1995) High-resolution structure of the catalytic domain of avian sarcoma virus integrase, *J. Mol. Biol. 253*, 333−346.
10. Chen, J. C., Krucinski, J., Miercke, L. J., Finer-Moore, J. S., Tang, A. H., Leavitt, A. D., and Stroud, R. M. (2000) Crystal structure of the HIV-1 integrase catalytic core and C-terminal domains: A model for viral DNA binding, *Proc. Natl. Acad. Sci. U.S.A. 97*, 8233−8238.
11. Chen, Z., Yan, Y., Munshi, S., Li, Y., Zugay-Murphy, J., Xu, B., Witmer, M., Felock, P., Wolfe, A., Sardana, V., Emini, E. A., Hazuda, D., and Kuo, L. C. (2000) X-ray structure of simian immunodeficiency virus integrase containing the core and C-terminal domain (residues 50−293): An initial glance of the viral DNA binding platform, *J. Mol. Biol. 296*, 521−533.
12. Yang, Z. N., Mueser, T. C., Bushman, F. D., and Hyde, C. C. (2000) Crystal structure of an active two-domain derivative of Rous sarcoma virus integrase, *J. Mol. Biol. 296*, 535−548.
13. Wang, J. Y., Ling, H., Yang, W., and Craigie, R. (2001) Structure of a two-domain fragment of HIV-1 integrase: Implications for domain organization in the intact protein, *EMBO J. 20*, 7333−7343.
14. Kulkosky, J., Jones, K. S., Katz, R. A., Mack, J. P., and Skalka, A. M. (1992) Residues critical for retroviral integrative recombination in a region that is highly conserved among retroviral/retrotransposon integrases and bacterial insertion sequence transposases, *Mol. Cell. Biol. 12*, 2331−2338.
15. Jenkins, T. M., Engelman, A., Ghirlando, R., and Craigie, R. (1996) A soluble active mutant of HIV-1 integrase: Involvement of both the core and carboxyl-terminal domains in multimerization, *J. Biol. Chem. 271*, 7712−7718.
16. Heuer, T. S., and Brown, P. O. (1998) Photo-cross-linking studies suggest a model for the architecture of an active human immunodeficiency virus type 1 integrase-DNA complex, *Biochemistry 37*, 6667−6678.
17. Gao, K., Butler, S. L., and Bushman, F. (2001) Human immunodeficiency virus type 1 integrase: Arrangement of protein domains in active cDNA complexes, *EMBO J. 20*, 3565−3576.
18. Clegg, R. M. (1992) Fluorescence resonance energy transfer and nucleic acids, *Methods Enzymol. 211*, 353−405.
19. Heyduk, T., and Heyduk, E. (2002) Molecular beacons for detecting DNA binding proteins, *Nat. Biotechnol. 20*, 171−176.
20. Vora, A., and Grandgenett, D. P. (2001) DNase protection analysis of retrovirus integrase at the viral DNA ends for full-site integration in vitro, *J. Virol. 75*, 3556−3567.
21. Chiu, R., and Grandgenett, D. P. (2003) Molecular and genetic determinants of Rous sarcoma virus integrase for concerted DNA integration, *J. Virol. 77*, 6482−6492.
22. Vora, A., Bera, S., and Grandgenett, D. (2004) Structural organization of avian retrovirus integrase in assembled intasomes mediating full-site integration, *J. Biol. Chem. 279*, 18670−18678.
23. McCord, M., Stahl, S. J., Mueser, T. C., Hyde, C. C., Vora, A. C., and Grandgenett, D. P. (1998) Purification of recombinant Rous sarcoma virus integrase possessing physical and catalytic properties similar to virion-derived integrase, *Protein Expression Purif. 14*, 167−177.
24. Vora, A. C., and Grandgenett, D. P. (1995) Assembly and catalytic properties of retrovirus integrase DNA complexes capable of efficiently performing concerted integration, *J. Virol. 69*, 7483−7488.

25. Vora, A. C., Chiu, R., McCord, M., Goodarzi, G., Stahl, S. J., Mueser, T. C., Hyde, C. C., and Grandgenett, D. P. (1997) Avian retrovirus U3 and U5 DNA inverted repeats. Role of nonsymmetrical nucleotides in promoting full-site integration by purified virion and bacterial recombinant integrases, *J. Biol. Chem. 272*, 23938−23945.
26. Chiu, R., and Grandgenett, D. P. (2000) Avian retrovirus DNA internal attachment site requirements for full-site integration in vitro, *J. Virol. 74*, 8292−8298.
27. Aiyar, A., Hindmarsh, P., Skalka, A. M., and Leis, J. (1996) Concerted integration of linear retroviral DNA by the avian sarcoma virus integrase in vitro: Dependence on both long terminal repeat termini, *J. Virol. 70*, 3571−3580.
28. Moreau, K., Faure, C., Verdier, G., and Ronfort, C. (2002) Analysis of conserved and non-conserved amino acids critical for ALSV (Avian leukemia and sarcoma viruses) integrase functions in vitro, *Arch. Virol. 147*, 1761−1778.
29. Moreau, K., Faure, C., Violot, S., Gouet, P., Verdier, G., and Ronfort, C. (2004) Mutational analyses of the core domain of avian leukemia and sarcoma viruses integrase: Critical residues for concerted integration and multimerization, *Virology 318*, 566−581.
30. Zhou, H., Rainey, G. J., Wong, S. K., and Coffin, J. M. (2001) Substrate sequence selection by retroviral integrase, *J. Virol. 75*, 1359−1370.
31. Esposito, D., and Craigie, R. (1998) Sequence specificity of viral end DNA binding by HIV-1 integrase reveals critical regions for protein-DNA interaction, *EMBO J. 17*, 5832−5843.
32. Ellison, V., and Brown, P. O. (1994) A stable complex between integrase and viral DNA ends mediates human immunodeficiency virus integration in vitro, *Proc. Natl. Acad. Sci. U.S.A. 91*, 7316−7320.
33. Brin, E., Yi, J., Skalka, A. M., and Leis, J. (2000) Modeling the late steps in HIV-1 retroviral integrase-catalyzed DNA integration, *J. Biol. Chem. 275*, 39287−39295.
34. McCord, M., Chiu, R., Vora, A. C., and Grandgenett, D. P. (1999) Retrovirus DNA termini bound by integrase communicate in trans for full-site integration in vitro, *Virology 259*, 392−401.
35. Murphy, J. E., and Goff, S. P. (1992) A mutation at one end of Moloney murine leukemia virus DNA blocks cleavage of both ends by the viral integrase in vivo, *J. Virol. 66*, 5092−5095.
36. Murphy, J. E., De Los Santos, T., and Goff, S. P. (1993) Mutational analysis of the sequences at the termini of the Moloney murine leukemia virus DNA required for integration, *Virology 195*, 432−440.
37. Asante-Appiah, E., Seeholzer, S. H., and Skalka, A. M. (1998) Structural determinants of metal-induced conformational changes in HIV-1 integrase, *J. Biol. Chem. 273*, 35078−35087.
38. Espeseth, A. S., Felock, P., Wolfe, A., Witmer, M., Grobler, J., Anthony, N., Egbertson, M., Melamed, J. Y., Young, S., Hamill, T., Cole, J. L., and Hazuda, D. J. (2000) HIV-1 integrase inhibitors that compete with the target DNA substrate define a unique strand transfer conformation for integrase, *Proc. Natl. Acad. Sci. U.S.A. 97*, 11244−11249.
39. Hazuda, D. J., Felock, P., Witmer, M., Wolfe, A., Stillmock, K., Grobler, J. A., Espeseth, A., Gabryelski, L., Schleif, W., Blau, C., and Miller, M. D. (2000) Inhibitors of strand transfer that prevent integration and inhibit HIV-1 replication in cells, *Science 287*, 646−650.
40. Brown, H. E., Chen, H., and Engelman, A. (1999) Structure-based mutagenesis of the human immunodeficiency virus type 1 DNA attachment site: Effects on integration and cDNA synthesis, *J. Virol. 73*, 9011−9020.
41. Chen, H., and Engelman, A. (2000) Characterization of a replication-defective human immunodeficiency virus type 1 att site mutant that is blocked after the 3′ processing step of retroviral integration, *J. Virol. 74*, 8188−8193.
42. Khan, E., Mack, J. P., Katz, R. A., Kulkosky, J., and Skalka, A. M. (1991) Retroviral integrase domains: DNA binding and the recognition of LTR sequences, *Nucleic Acids Res. 19*, 851−860.
43. Pemberton, I. K., Buckle, M., and Buc, H. (1996) The metal ion-induced cooperative binding of HIV-1 integrase to DNA exhibits a marked preference for Mn(II) rather than Mg(II), *J. Biol. Chem. 271*, 1498−1506.
44. Craigie, R. (2002) Retroviral DNA Integration, in *Mobil DNA II* (Craig, N. L., Craigie, R., Gellert, M., and Lambowitz, A. M., Eds.) pp 613−630, American Society for Microbiology, Washington, DC.
45. Wang, T., Balakrishnan, M., and Jonsson, C. B. (1999) Major and minor groove contacts in retroviral integrase-LTR interactions, *Biochemistry 38*, 3624−3632.
46. Wei, S. Q., Mizuuchi, K., and Craigie, R. (1997) A large nucleoprotein assembly at the ends of the viral DNA mediates retroviral DNA integration, *EMBO J. 16*, 7511−7520.
47. Chen, H., Wei, S. Q., and Engelman, A. (1999) Multiple integrase functions are required to form the native structure of the human immunodeficiency virus type I intasome, *J. Biol. Chem. 274*, 17358−17364.
48. Selvin, P. R. (2002) Principles and biophysical applications of lanthanide-based probes, *Annu. Rev. Biophys. Biomol. Struct. 31*, 275−302.

BI0508340